Electrical Power and Energy Systems 156 (2024) 109718

Contents lists available at ScienceDirect

International Journal of Electrical Power and Energy Systems

journal homepage: www.elsevier.com/locate/ijepes

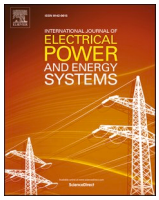

# Predictive direct control strategy of unified power quality conditioner based on power angle control

Guifeng Wang, Zewen Wu, Zhan Liu *

*School of Electrical Engineering and Automation, Jiangsu Normal University, Xuzhou 221116, China*

ARTICLE INFO

*Keywords:*
Finite control set model predictive control
Power angle control
Power quality
Unified power quality conditioner
Power coordination
Reactive power compensation

ABSTRACT

The unified power quality conditioner (UPQC), based on power angle control (PAC), addresses the power distribution issue and enhances equipment utilization between two active power filters (APF) of UPQC by employing conventional linear control algorithms that have complex control structures and exhibit challenges in adjusting controller parameters and control delays. This study proposes a UPQC predictive direct control strategy based on power angle control (PDCS-PAC). We combine the direct control strategy with the finite control set model predictive control (FCS-MPC) to establish the UPQC finite set model predictive direct control system model in the *dq* coordinate system. This approach simplifies the controller structure and alleviates the control algorithm's complexity. Based on a detailed analysis of the PAC mechanism, an instantaneous power angle determination method is proposed based on the reactive power equalization technique, and a predictive direct control strategy given the current generation mechanism is constructed for the series and shunt sides of the UPQC, considering the active power balance of the UPQC system and the principle of constant load fundamental voltage amplitude. Finally, we construct a simulation platform and a laboratory prototype to validate the feasibility and efficacy of the proposed control strategy.

## 1. Introduction

The ubiquity of distributed power sources and non-linear loads [1] has increased the power systems' susceptibility to power quality issues, such as current distortions and voltage disturbances [2]. To address these challenges [3], various power electronics compensation devices have been proposed [4,5]. Among them, the unified power quality condition (UPQC) can compensate for harmonic currents and harmonic voltages at the network's load side and suppress disturbances such as voltage dips, drops, and fluctuations [6]. The UPQC combines the advantages of a series active power filter (SAPF) and parallel active power filter (PAPF) [7], rendering it ideal for comprehensively addressing power quality issues at the grid and customer sides [8].

Based on the UPQC control method and the electrical quantity being regulated [9], UPQC control strategies are categorized into indirect control [10] and direct control [11,12]. The direct control strategy considers the fundamental components of voltage and current in the control object, bypassing harmonic component detection. This mechanism allows transformation to a fluctuation-free direct current (DC) component in the *dq* coordinate system and easy attainment of static-free control using proportional-integral (PI) controllers. Regardless of the chosen control strategy, the control objectives are achieved through SAPF compensation of the voltage difference between the grid and the load, and PAPF provision of load reactive power demand and compensation of harmonic currents. Consequently, in conventional UPQC control strategies, the PAPF often operates in a high load state while fulfilling load reactive power demand and compensating for harmonic current, while the SAPF remains mostly idle and does not contribute to load reactive power compensation.

Recently, researchers have proposed the phase angle coordination (PAC) technique to optimize the power balance between SAPF and PAPF [13,14]. PAC achieves global power coordination control of UPQC systems by integrating a certain phase angle shift between the load voltage and grid voltage to regulate SAPF to process part of the reactive power [15]. This approach reduces the required installation capacity and enhances equipment utilization [16]. Based on the UPQC reactive power flow theory analysis, a study established a multi-intelligent dynamic coordinated control mechanism [17], using SAPF instead of PAPF for full reactive power compensation, while reserving PAPF for harmonic compensation without considering power balance between the two

* Corresponding author.
*E-mail address:* liuzhan_cumt@163.com (Z. Liu).

https://doi.org/10.1016/j.ijepes.2023.109718
Received 31 March 2023; Received in revised form 14 November 2023; Accepted 8 December 2023
Available online 21 December 2023

converters. Subsequently, some studies have realized the reactive power sharing function between active power filters (APFs) on both sides by controlling SAPF voltage, allowing it to provide part of the load reactive power demand [18]. However, this approach does not address voltage transient change compensation and reactive power through SAPF simultaneously. Reference [19] proposes a compensation strategy for power coordinated distribution to maintain SAPF's operating voltage at its rated value to offload PAPF to the maximum extent. Nevertheless, PAPF still provides the load's reactive power, which strains SAPF when the load's reactive power demand exceeds PAPf's capacity. To address load current harmonics and grid voltage comprehensively [20], a detailed analysis of the reactive power coordination control mechanism based on the power angle control strategy is presented. This approach mitigates active loop current between SAPF and PAPF, minimizes power losses, optimizes SAPF's role, and alleviates prolonged overloads and heavy load issues of the PAPF. However, this technique relies on a dual closed-loop control system, which introduces multiple linear controllers, leading to challenges in parameter rectifications and increasing algorithm complexity and system delays.

Therefore, it is crucial to enhance the UPQC control strategy's compensation performance, eliminate complex parameter rectification links, and achieve power balance on both converter sides. Fractional-order control strategy with model predictive control (FCS-MPC) offers an appealing solution due to its intuitive and easy-to-understand modeling, absence of PID controllers and PWM modulators, and simple control structure [21]. This approach has the potential to further enhance the UPQC control system [22].

Recent applications of FCS-MPC in power quality control have primarily focused on active power filters, centering on algorithm refinement to reduce prediction computations [23], expanding the range of selectable vectors through virtual vector synthesis to improve system control performance [24], designing systems for specialized applications [25], and investigating different topologies [26]. However, research on UPQC control strategies employing FCS-MPC remains relatively scarce and is primarily at the stage of program feasibility verification [27,31]. Compared to conventional PI closed-loop control systems, the UPQC power quality disturbance compensation strategy based on FCS-MPC minimizes the tedium of parameter tuning and eliminates linear controllers and modulation techniques. However, due to the indirect control principles, the power quality compensation effect is influenced by the harmonic detection link [28,29]. To address this concern, a direct prediction compensation strategy based on FCS-MPC has been proposed [30]. This approach simplifies the UPQC controller structure and enhances system control performance by constructing a prediction model within the coordinate system. However, this method relies on vector operations and does not address the power balancing problem of SAPF and PAPF.

To address the challenges in existing approaches, this study proposes a UPQC predictive direct control strategy based on Power Angle Control (PDCS-PAC) as follows.

1) A UPQC predictive direct control strategy based on PAC in the *dq* coordinate system is implemented, simplifying the controller structure.
2) The instantaneous power angle values of the PDCS-PAC are determined using the reactive power averaging method.
3) Following an analysis of the PAC control mechanism, a predictive direct control approach for the given current generation for SAPF and PAPF is established. This approach considers the active power balance within the UPQC system and maintains the constant amplitude principle of the load fundamental voltage.

The remaining paper is organized as follows. Section 2 presents the system modeling of PDCS-PAC-based UPQC. Section 3 elaborates on the given current generation mechanism of PDCS-PAC-based UPQC. Section 4 provides the simulation and experimental analyses of the proposed strategy. Finally, Section 5 outlines the contributions of this study.

## 2. System modelling of UPQC based on PDCS-PAC

### 2.1. Brief analysis of the PAC method

The UPQC topology for a two-level, three-phase, three-wire system is illustrated in Fig. 1. The figure depicts the supply voltage ($u_{sa}$, $u_{sb}$, and $u_{sc}$), the load voltage ($u_{La}$, $u_{Lb}$, and $u_{Lc}$), the SAPF output voltage ($u_{a1}$, $u_{b1}$, and $u_{c1}$), the PAPF output voltage ($u_{a2}$, $u_{b2}$, and $u_{c2}$), the series transformer grid compensation voltage ($u_{ca}$, $u_{cb}$, and $u_{cc}$), the series transformer secondary side current ($i_{ca1}$, $i_{cb1}$, and $i_{cc1}$), the SAPF output current ($i_{a1}$, $i_{b1}$, and $i_{c1}$), the PAPF output current ($i_{a2}$, $i_{b2}$, and $i_{c2}$),.the PAPF load compensation current ($i_{ca2}$, $i_{cb2}$, and $i_{cc2}$), the supply current ($i_{sa}$, $i_{sb}$, and $i_{sc}$), and the load current ($i_{La}$, $i_{Lb}$, and $i_{Lc}$). In the figure, $C_1$ and $L_1$ denote SAPF's filter capacitor and filter inductor, respectively; $C_2$ and $L_2$ signify PAPF's filter capacitor and filter inductor, respectively; $C$ represents the UPQC DC side energy storage capacitor; and $u_{DC}$ is the voltage across $C$.

The PAC control's schematic diagram is depicted in Fig. 2. The figure shows the supply voltage and current ($U_s$ and $I_s$), the load voltage and current ($U_L$ and $I_L$), the load voltage and current by the PAC ($U_L^{'}$ and $I_L^{'}$), the compensation currents of the PAPF without and with the PAC ($I_{sh}$ and $I_{sh}^{'}$), the supply voltage and current during voltage fluctuations ($U_s^{'}$ and $I_s^{'}$), and the compensation voltage of the SAPF ($U_{se}$). In addition, $\delta$ denotes the power angle control between $U_s$ and $U_L^{'}$; $\varphi_{se}$ and $\varphi_{sh}^{'}$ signify the angles between $U_{se}$ and $U_s$ and between $I_{sh}^{'}$ and $U_L^{'}$, respectively; $\varphi$ represents the power factor angle; $U$ and $I$ are the root mean square values of the desired load voltage and load current, respectively.

Without PAC, the PAPF fulfills the load's reactive power demand by injecting the compensation current $I_{sh}$. In this case, the PAPF supplies all the reactive power required by the load. In contrast, the PAC control strategy involves the SAPF injecting voltage through the series transformer, causing a shift in the load voltage from $U_L$ to $U_L^{'}$ and a certain portion of reactive power to route through the SAPF. Therefore, the SAPF contributes to the load's reactive power. Concurrently, the load current $I_L$ shifts to $I_L^{'}$, necessitating the PAPF to inject compensation current $I_{sh}^{'}$ to ensure that no additional active power is provided on the supply side. The indirect UPQC control achieves the desired displacement between the network-side voltage and the load voltage by introducing a precisely angled fundamental frequency voltage to both ends of the coupling transformer [17]. In contrast, the UPQC control strategy based on direct control allows PAPF's direct control of the load voltage [19]. To optimize SAPF utilization and alleviate prolonged heavy PAPF operation, the PDCS-PAC modifies the coordinate transformation angle in the PAPF prediction model and the given current generation mechanism to control the phase angle difference $\delta$ between the load voltage and the grid voltage.

### 2.2. SAPF modeling based on PDCS-PAC

The mathematical model for SAPF in the *dq* coordinate system is

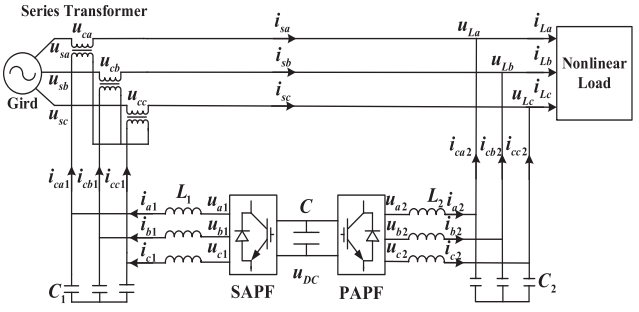


**Fig. 1.** Topology structure of UPQC.

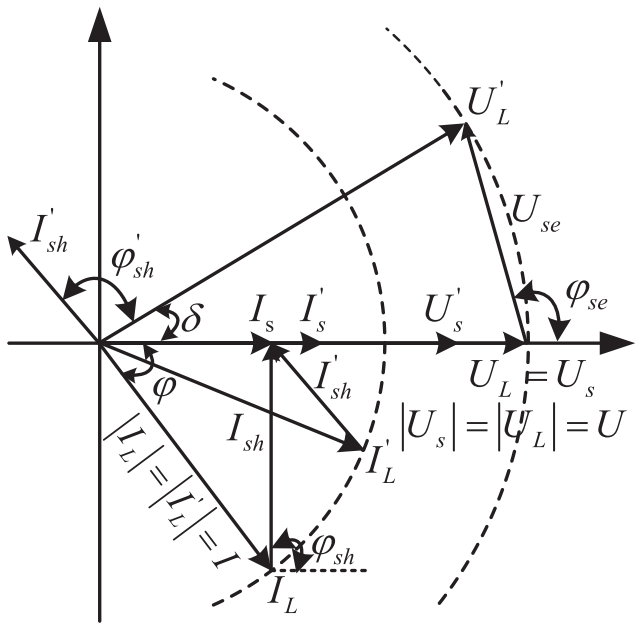


**Fig. 2.** PAC control's schematic diagram.

expressed as

$$\frac{d}{dt}\begin{bmatrix} i_{d1} \\ i_{q1} \end{bmatrix} = \begin{bmatrix} 0 & \omega \\ -\omega & 0 \end{bmatrix}\begin{bmatrix} i_{d1} \\ i_{q1} \end{bmatrix} + \frac{1}{L_1}\begin{bmatrix} u_{d1} - u_{cd} \\ u_{q1} - u_{cq} \end{bmatrix} \tag{1}$$

where $i_{d1}$ and $i_{q1}$, $u_{cd}$ and $u_{cq}$, and $u_{d1}$ and $u_{q1}$ denote the $d$- and $q$-axes components of the SAPF output currents $i_{a1}$, $i_{b1}$, and $i_{c1}$, the series transformer grid compensation voltages $u_{ca}$, $u_{cb}$, and $u_{cc}$, and the SAPF output voltages $u_{a1}$, $u_{b1}$, and $u_{c1}$ following the $M_1$ transformation, respectively; $L_1$ represents the filter inductance of the SAPF; and $\omega$ signifies the grid angular frequency.

$$M_1 = \frac{2}{3}\begin{bmatrix} \cos\theta_1 & \cos(\theta_1 - \frac{2\pi}{3}) & \cos(\theta_1 + \frac{2\pi}{3}) \\ -\sin\theta_1 & -\sin(\theta_1 - \frac{2\pi}{3}) & -\sin(\theta_1 + \frac{2\pi}{3}) \end{bmatrix} \tag{2}$$

where $\theta_1 = \omega t$.

A discretization of (1) yields the following SAPF prediction model.

$$\begin{bmatrix} i_{d1}(k+1) \\ i_{q1}(k+1) \end{bmatrix} = \begin{bmatrix} 1 & T_s\omega \\ -T_s\omega & 1 \end{bmatrix}\begin{bmatrix} i_{d1}(k) \\ i_{q1}(k) \end{bmatrix} + \frac{T_s}{L_1}\begin{bmatrix} u_{d1} - u_{cd}(k) \\ u_{q1} - u_{cq}(k) \end{bmatrix} \tag{3}$$

where $T_s$ denotes the discretization period.

This study uses a control delay compensation method to compensate for the delay effect generated by the digital signal controller [32]. Combining (3) with the SAPF optimal voltage vectors $u_{od1}$ and $u_{oq1}$ at moment $k$, the control delay compensation current $i_{kd1}(k+1)$ and $i_{kq1}(k+1)$ at moment $k+1$ are derived as:

$$\begin{bmatrix} i_{kd1}(k+1) \\ i_{kq1}(k+1) \end{bmatrix} = \begin{bmatrix} 1 & T_s\omega \\ -T_s\omega & 1 \end{bmatrix}\begin{bmatrix} i_{d1}(k) \\ i_{q1}(k) \end{bmatrix} + \frac{T_s}{L_1}\begin{bmatrix} u_{od1} - u_{cd}(k) \\ u_{oq1} - u_{cq}(k) \end{bmatrix} \tag{4}$$

Using the eight voltage fundamental vectors generated by the switching state [30], with the SAPF prediction model, the predicted current values $i^n_{cd1}(k+2)$ and $i^n_{cq1}(k+2)$ at moment $k+2$ are computed as follows:

$$\begin{bmatrix} i^n_{cd1}(k+2) \\ i^n_{cq1}(k+2) \end{bmatrix} = \begin{bmatrix} 1 & T_s\omega \\ -T_s\omega & 1 \end{bmatrix}\begin{bmatrix} i_{kd1}(k+1) \\ i_{kq1}(k+1) \end{bmatrix} + \frac{T_s}{L_1}\begin{bmatrix} u_{d1}(k+1) - u_{cd}(k+1) \\ u_{q1}(k+1) - u_{cq}(k+1) \end{bmatrix} \tag{5}$$

where $n = 1 \sim 8$.

Since the UPQC requires time to execute the FCS-MPC algorithm, hindering the timely and precise compensation of the harmonic components, addressing the time delay issue associated with the FCS-MPC is imperative. This study employs two Lagrangian second-order extrapolations to compensate for the time delay for the given current:

$$\begin{bmatrix} i^p_{scd}(k+2) \\ i^p_{scq}(k+2) \end{bmatrix} = 6\begin{bmatrix} i^*_{sd1}(k) \\ i^*_{sq1}(k) \end{bmatrix} - 8\begin{bmatrix} i^*_{sd1}(k-1) \\ i^*_{sq1}(k-1) \end{bmatrix} + \begin{bmatrix} i^*_{sd1}(k-2) \\ i^*_{sq1}(k-2) \end{bmatrix} \tag{6}$$

where $i^*_{sd1}(k\text{-}2)$, $i^*_{sq1}(k\text{-}2)$, $i^*_{sd1}(k\text{-}1)$, $i^*_{sq1}(k\text{-}1)$, $i^*_{sd1}(k)$, $i^*_{sq1}(k)$, $i^p_{scd}(k+2)$, and $i^p_{scq}(k+2)$ denotes the given currents at $k$–2, $k$–1, $k$, and $k+2$, respectively.

The SAPF current prediction at moment $k+2$ is evaluated by substituting $i^p_{scd}$, $i^p_{scq}$, $i^n_{cd1}$ and $i^n_{cq1}$ into the cost function $g^n{}_1$:

$$g^n_1 = \left(i^p_{scd}(k+2) - i^n_{cd1}(k+2)\right)^2 + \left(i^p_{scq}(k+2) - i^n_{cq1}(k+2)\right)^2 \tag{7}$$

The switching state $N_1$ that minimizes the switching state $g^n{}_1$ of the SAPF output at moment $k+2$ is determined as:

$$N_1 = \underset{n}{\operatorname{argming}}{}^n_1(k+2) \tag{8}$$

### 2.3. PAPF modeling based on PDCS-PAC

The mathematical model for PAPF in the $dq$ coordinate system is

$$\frac{d}{dt}\begin{bmatrix} i_{d2} \\ i_{q2} \end{bmatrix} = \begin{bmatrix} 0 & \omega \\ -\omega & 0 \end{bmatrix}\begin{bmatrix} i_{d2} \\ i_{q2} \end{bmatrix} + \frac{1}{L_2}\begin{bmatrix} u_{d2} - u_{Ld} \\ u_{q2} - u_{Lq} \end{bmatrix} \tag{9}$$

where $i_{d2}$ and $i_{q2}$, $u_{Ld}$ and $u_{Lq}$, and $u_{d2}$ and $u_{q2}$ denote the $d$- and $q$-axes components of the PAPF output currents $i_{a2}$, $i_{b2}$, and $i_{c2}$, the load voltages $u_{La}$, $u_{Lb}$, and $u_{Lc}$, the PAPF output voltages $u_{a2}$, $u_{b2}$, and $u_{c2}$ following the $M_2$ transformation, respectively; $L_2$ signifies the filter inductor of the PAPF.

$$M_2 = \frac{2}{3}\begin{bmatrix} \cos\theta_2 & \cos(\theta_2 - \frac{2\pi}{3}) & \cos(\theta_2 + \frac{2\pi}{3}) \\ -\sin\theta_2 & -\sin(\theta_2 - \frac{2\pi}{3}) & -\sin(\theta_2 + \frac{2\pi}{3}) \end{bmatrix} \tag{10}$$

where $\theta_2 = \theta_1 + \delta$.

A discretization of (9) yields the PAPF prediction model.

$$\begin{bmatrix} i_{d2}(k+1) \\ i_{q2}(k+1) \end{bmatrix} = \begin{bmatrix} 1 & T_s\omega \\ -T_s\omega & 1 \end{bmatrix}\begin{bmatrix} i_{d2}(k) \\ i_{q2}(k) \end{bmatrix} + \frac{T_s}{L_2}\begin{bmatrix} u_{d2} - u_{Ld}(k) \\ u_{q2} - u_{Lq}(k) \end{bmatrix} \tag{11}$$

Combining (11) with the PAPF optimal voltage vectors $u_{od2}$ and $u_{oq2}$ at moment $k$, the control delay compensation current $i_{kd2}(k+1)$ and $i_{kq2}(k+1)$ at moment $k+1$ are obtained as follows:

$$\begin{bmatrix} i_{kd2}(k+1) \\ i_{kq2}(k+1) \end{bmatrix} = \begin{bmatrix} 1 & T_s\omega \\ -T_s\omega & 1 \end{bmatrix}\begin{bmatrix} i_{d2}(k) \\ i_{q2}(k) \end{bmatrix} + \frac{T_s}{L_2}\begin{bmatrix} u_{od2} - u_{Ld}(k) \\ u_{oq2} - u_{Lq}(k) \end{bmatrix} \tag{12}$$

Utilizing the eight voltage fundamental vectors generated by the switching state and integrating them with the PAPF prediction model, the predicted currents $i^n_{cd2}(k+2)$ and $i^n_{cq2}(k+2)$ at moment $k+2$ are derived as follows:

$$\begin{bmatrix} i^n_{cd2}(k+2) \\ i^n_{cq2}(k+2) \end{bmatrix} = \begin{bmatrix} 1 & T_s\omega \\ -T_s\omega & 1 \end{bmatrix}\begin{bmatrix} i_{kd2}(k+1) \\ i_{kq2}(k+1) \end{bmatrix} + \frac{T_s}{L_2}\begin{bmatrix} u_{d2}(k+1) - u_{Ld}(k+1) \\ u_{q2}(k+1) - u_{Lq}(k+1) \end{bmatrix} \tag{13}$$

Delayed compensation for a given current is addressed using two Lagrangian second-order extrapolations:

$$\begin{bmatrix} i^p_{Lbd}(k+2) \\ i^p_{Lbq}(k+2) \end{bmatrix} = 6\begin{bmatrix} i^*_{Ld2}(k) \\ i^*_{Lq2}(k) \end{bmatrix} - 8\begin{bmatrix} i^*_{Ld2}(k-1) \\ i^*_{Lq2}(k-1) \end{bmatrix} + \begin{bmatrix} i^*_{Ld2}(k-2) \\ i^*_{Lq2}(k-2) \end{bmatrix} \tag{14}$$

where $i^*_{Ld2}(k\text{-}2)$,$i^*_{Lq2}(k\text{-}2)$,$i^*_{Ld2}(k\text{-}1)$,$i^*_{Lq2}(k\text{-}1)$,$i^*_{Ld2}(k)$,$i^*_{Lq2}(k)$,

$i^p_{Lbd}(k+2)$, and $i^p_{Lbq}(k+2)$ represent the given currents corresponding to $k$–2, $k$–1, $k$, and $k+2$, respectively.

By substituting $i^p_{Lbd}$, $i^p_{Lbq}$, $i^n_{cd2}$ and $i^n_{cq2}$ into the cost function $g^n{}_2$, we can derive the PAPF current prediction at moment $k+2$ as follows:

$$g^n_2 = \left(i^p_{Lbd}(k+2) - i^n_{cd2}(k+2)\right)^2 + \left(i^p_{Lbq}(k+2) - i^n_{cq2}(k+2)\right)^2 \tag{15}$$

The switching state $N_2$, which minimizes the switching state $g^n{}_2$ of the PAPF output at moment $k+2$ is obtained as:

$$N_2 = \underset{n}{\arg\min} g^n_2(k+2) \tag{16}$$

## 3. The current generation mechanism of UPQC based on PDCS-PAC

### 3.1. Instantaneous power angle δ determination of UPQC based on PDCS-PAC

Following an in-depth analysis of power flow and the derived correlation equations for the converters on both sides of the UPQC controlled by PAC [15], Reference [33] provides the expression for the fundamental reactive power $Q_{SAPFf}$ of SAPF under all working conditions:

$$Q_{SAPFf} = \frac{UI}{f}\sin\delta\cos\varphi \tag{17}$$

where $f$ denotes the ratio of the disturbed supply voltage $U_s^{'}$ root mean square to the normal voltage $U_s^{'}$ ($f = U^{'}/U$).

Ideally, the active power supplied by the grid $P_{sf}$ and required by the load $P_{Lf}$ are identical. Therefore, the power angle $\delta$ can be expressed as:

$$\delta = \sin^{-1}\left[\frac{fQ_{SAPFf}}{UI\cos\varphi}\right] = \sin^{-1}\left[\frac{fQ_{SAPFf}}{P_{sf}}\right] = \sin^{-1}\left[\frac{fQ_{SAPFf}}{P_{Lf}}\right] \tag{18}$$

Based on the reactive power equalization method [20], the SAPF and PAPF are designed to ensure equal load reactive power sharing, i.e. $Q_{SAPFf} = Q_{PAPFf} = 0.5Q_{Lf}$. The instantaneous power angle $\delta$ is determined by combining (18).

$$\delta = \sin^{-1}\left[\frac{fQ_{Lf}}{2P_{Lf}}\right] \tag{19}$$

To ascertain the instantaneous fundamental components $P_{Lf}$ and $Q_{Lf}$ of the active and reactive power of the load, the load's three-phase voltage and current are transformed into the $dq$ coordinate system following the principle of constant power transformation.

$$\begin{bmatrix} u_{Ldp} & u_{Lqp} \end{bmatrix}^T = \sqrt{\frac{3}{2}} M_1 \begin{bmatrix} u_{La} & u_{Lb} & u_{Lc} \end{bmatrix}^T \tag{20}$$

$$\begin{bmatrix} i_{Ldp} & i_{Lqp} \end{bmatrix}^T = \sqrt{\frac{3}{2}} M_1 \begin{bmatrix} i_{La} & i_{Lb} & i_{Lc} \end{bmatrix}^T \tag{21}$$

where $u_{Ldp}$, $u_{Lqp}$, $i_{Ldp}$, and $i_{Lqp}$ denote the $d$- and $q$-axes components of the load voltage and current, respectively, following the constant power transformation.

The instantaneous fundamental components $u_{Ldpf}$, $u_{Lqpf}$, $i_{Ldpf}$, and $i_{Lqpf}$ of the load voltage and current are extracted using a low-pass filter (LPF). $P_{Lf}$ and $Q_{Lf}$ are attained by substituting the following equations.

$$\begin{bmatrix} P_{Lf} \\ Q_{Lf} \end{bmatrix} = \begin{bmatrix} u_{Ldpf} & u_{Lqpf} \\ -u_{Lqpf} & u_{Ldpf} \end{bmatrix} \begin{bmatrix} i_{Ldpf} \\ i_{Lqpf} \end{bmatrix} \tag{22}$$

The block diagram of the instantaneous power angle $\delta$ determination based on PDCS-PAC is illustrated in Fig. 3.

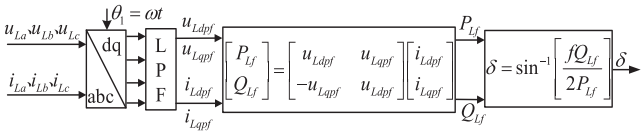


**Fig. 3.** Instantaneous $\delta$ determination.

### 3.2. Given the current's generation mechanism of SAPF based on PDCS-PAC

Utilizing the principle of active power balancing on the network and load sides [12], the $d$-axis feeder current $i^*_{sd1}$ of the SAPF combines the PI-regulated current $i_{DC}$ of the DC bus voltage and the current command feedforward $i_{sd}$. The $q$-axis feedthrough current $i^*_{sq1}$ is set to zero to ensure no reactive power input on the network side. In the PDCS-PAC-based UPQC, SAPF functions as a sinusoidal current source synchronized with the supply voltage to alleviate current quality issues and maintain a stable DC bus voltage while emitting some reactive power to relieve the reactive power burden on PAPF (Fig. 4).

In the $dq$ coordinate system, the $d$- and $q$-axes given currents $i^*_{sd1}$and $i^*_{sq1}$ of SAPF are computed as follows:

$$\begin{bmatrix} i^*_{sd1} \\ i^*_{sq1} \end{bmatrix} = \begin{bmatrix} i_{sd} + i_{DC} \\ 0 \end{bmatrix} \tag{23}$$

where $i_{DC}$ signifies the disparity between the DC bus reference voltage $u^*_{DC}$ and the actual voltage $u_{DC}$ regulated by the PI controller. $i_{DC}$ serves to compensate for system losses caused by filters and converters, balance the system power of UPQC, and stabilize the DC bus voltage.

The instantaneous fundamental components $u_{sdf}$, $u_{sqf}$, $u_{Ldf}$, $u_{Lqf}$, $i_{Ldf}$, and $i_{Lqf}$ of the load currents ($i_{La}$, $i_{Lb}$, and $i_{Lc}$), grid voltages ($u_{sa}$, $u_{sb}$, and $u_{sc}$) and load voltages ($u_{La}$, $u_{Lb}$, and $u_{Lc}$) are $M_1$ transformed, extracted using a LPF, and substituted into the following equation.

$$i_{sd} = \frac{u_{Ldf}i_{Ldf} + u_{Lqf}i_{Lqf}}{\sqrt{u^2_{sdf} + u^2_{sqf}}} \tag{24}$$

### 3.3. Given the current's generation mechanism of PDCS-PAC-based PAPF

The PI regulator minimizes load voltage fluctuations and maintains a sinusoidal load voltage with constant amplitude, following the constant amplitude principle of the compensated load voltage. This load voltage determines the given currents of the PAPF $i^*_{Ld2}$ and $i^*_{Lq2}$, the desired voltage, and the PAPF compensation current. The PDCS-PAC-based PAPF (Fig. 5) functions as a sinusoidal voltage source controlled in phase with the network side voltage to alleviate voltage quality issues. In the $dq$ coordinate system, the $d$- and $q$-axes desired voltages $u^*_{Ld}$ and $u^*_{Lq}$ are set to $220\sqrt{2}$ V and 0 V, respectively, to deliver the load voltage and suppress voltage harmonics, ensuring sinusoidal load voltage.

In the $dq$ coordinate system, the $d$- and $q$-axes, given currents $i^*_{Ld2}$ and $i^*_{Lq2}$ of PAPF, are determined as follows:

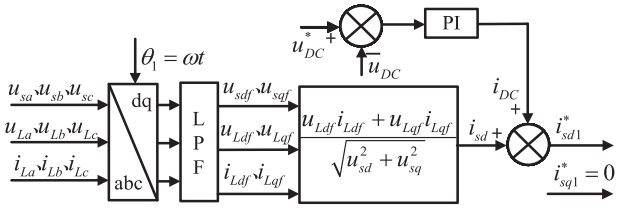


**Fig. 4.** The current generation mechanism of PDCS-PAC-based SAPF.

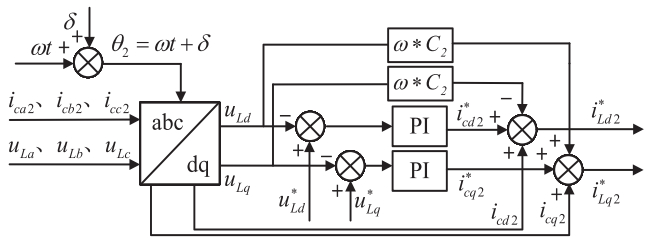


**Fig. 5.** The current generation mechanism of PDCS-PAC-based PAPF.

$$\begin{bmatrix} i^*_{Ld2} \\ i^*_{Lq2} \end{bmatrix} = \begin{bmatrix} i^*_{cd2} + i_{cd2} \\ i^*_{cq2} + i_{cq2} \end{bmatrix} + \begin{bmatrix} 0 & -\omega C_2 \\ \omega C_2 & 0 \end{bmatrix} \begin{bmatrix} u_{Ld} \\ u_{Lq} \end{bmatrix} \tag{25}$$

where $i^*_{cd2}$ and $i^*_{cq2}$ denote the PI-regulator-adjusted output values obtained by subtracting the desired voltage from the actual load voltage; $i_{cd2}$ and $i_{cq2}$ represent the *d*- and *q*-axes components of PAPF's load compensation currents ($i_{ca2}$, $i_{cb2}$, and $i_{cc2}$) after the $M_2$ transformation.

## 4. Simulation analysis

To assess the efficacy of the proposed PDCS-PAC control (Fig. 6), we employ MATLAB/Simulink for simulation and analysis. The circuit parameters of UPQC are listed in Table 1.

The simulation analysis encompasses the three-phase grid currents, the three-phase load voltages, the grid voltage and current phases, the DC bus voltage, and the reactive power under various working conditions. These conditions include a 15% voltage transient rise in the grid voltage at 0.1 s, a 15% voltage transient drop at 0.2 s, a voltage harmonic of about 12% at 0.3 s, and a sudden load change at 0.4 s.

### *4.1. Linear algorithms and predictive direct control strategy compensate for effects without PAC*

In Fig. 7, the linear algorithm and the predictive direct control strategy maintain the grid current sinusoidally. The linear algorithm exhibits a slower response near the power quality disturbance point due to coupling compensation issues. In contrast, the proposed UPQC predictive direct control strategy demonstrates a rapid stabilization of the compensated grid current near the disturbance point, ensuring grid current stability and a stronger compensation effect.

Grid voltage disturbance compensation (Fig. 8) depicts that the linear algorithm and the predictive direct control strategy can maintain the load voltage stable and sinusoidal characteristics, regardless of transient grid voltage variations, harmonics, or sudden load changes. The predictive direct control excels in compensation, exhibiting a superior control effect on load voltage during system disturbances compared to the linear algorithm.

Fig. 9 illustrates that the predictive direct control ensures that the

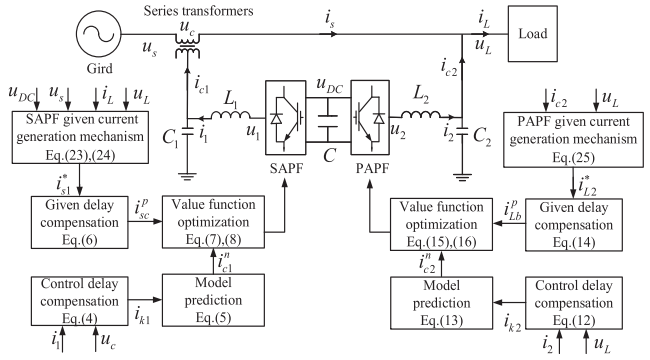


**Fig. 6.** Block diagram of PDCS-PAC-based UPQC system.

**Table 1**
UPQC circuit parameters.

| Simulation parameters | Numerical values |
|---|---|
| Grid voltage/frequency | 220 V/50 Hz |
| Series transformer ratios | 1:1 |
| Inductors and capacitors of SAPF | $L_1$ = 50 mH, $C_1$ = 0.2 μF |
| Inductors and capacitors of PAPF | $L_1$ = 4 mH, $C_1$ = 300 μF |
| Voltage and capacitance of DC bus | $u_{DC}$ = 800 V, $C$ = 5500 μF |
| FCS-MPC control period | $T_s$ = 70 μs |

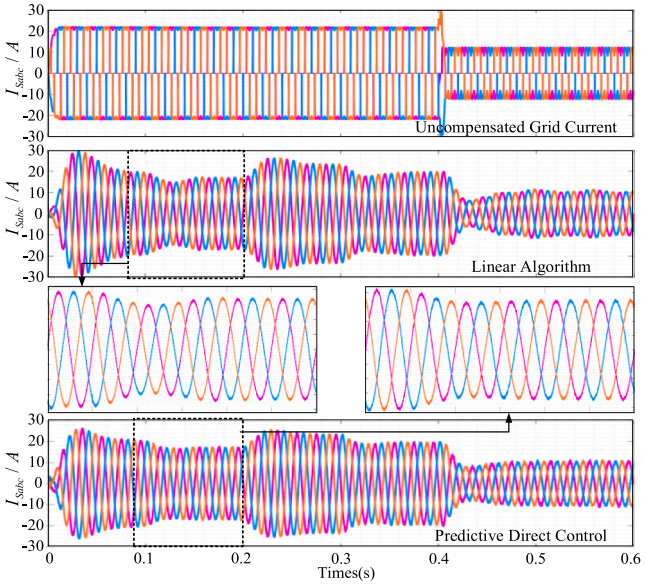


**Fig. 7.** Grid current of the two control algorithms under different working conditions.

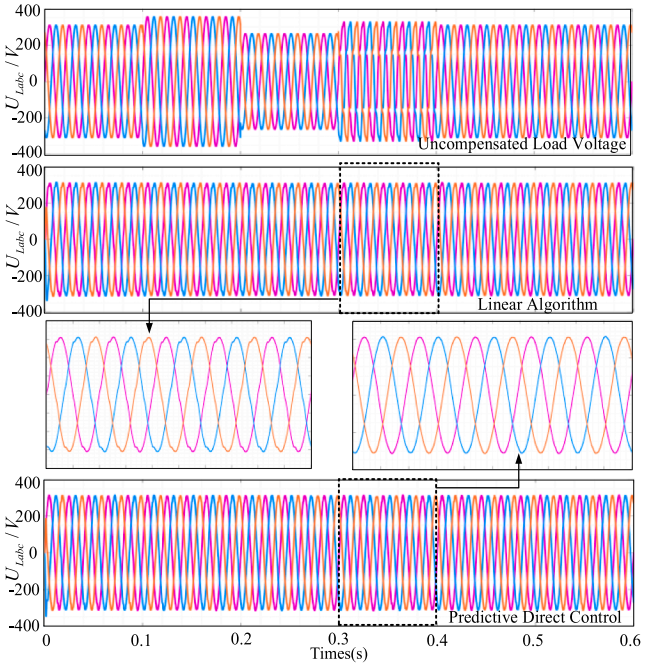


**Fig. 8.** Load voltage of two the control algorithms under different working conditions.

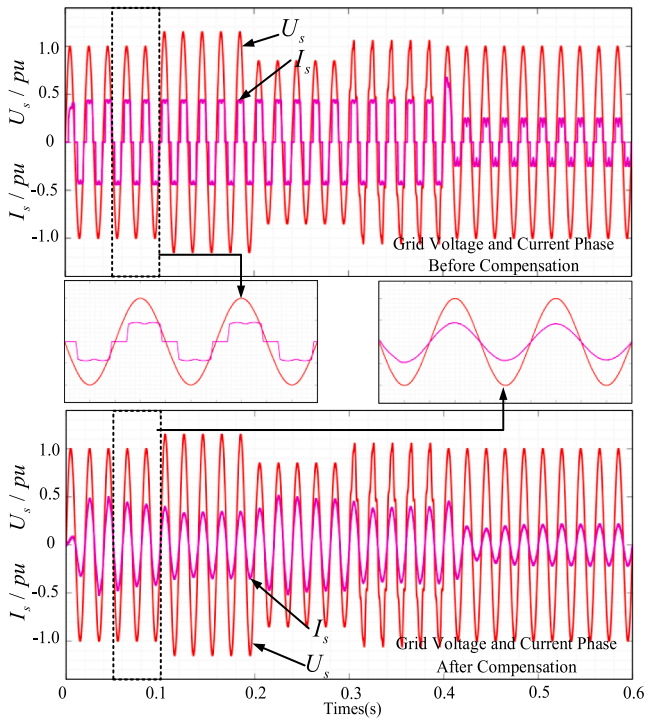


**Fig. 9.** Grid voltage and current phase.

power factor of the grid remains 1. Comparing the grid voltage and current phase before and after compensation indicates that the current waveform follows a sinusoidal pattern, aligning with the voltage waveform. This observation highlights the predictive direct control's effective harmonic current compensation characteristics.

The impact of the predictive direct control strategy on the DC bus voltage control is depicted in Fig. 10. Although the DC bus voltage fluctuates slightly during abrupt changes in operating conditions, it quickly regains stability using the proposed control strategy.

The reactive power waveform of the UPQC predictive direct control strategy without PAC (Fig. 11) indicates that PAPF supplies the reactive power required by the load under different operating conditions. Grid and SAPF emit minimal reactive power.

### 4.2. PDCS-PAC compensation effect

Simulation results of the PDCS-PAC compensation effect under various operating conditions are presented in Fig. 12 (a)–(d). The figures indicate that the PDCS-PAC strategy effectively maintains the stability of grid current, load voltage, and DC bus voltage, provides a robust compensation control effect when system disturbances occur, and ensures a grid-side power factor of 1. The proposed control strategy prompts the SAPF to contribute a portion of the reactive power required by the load under different operating conditions (Fig. 12 (e)). This enhancement enhances SAPF utilization and alleviates the reactive power burden on the PAPF.

Statistical data on the total harmonic distortion (THD) of the voltage

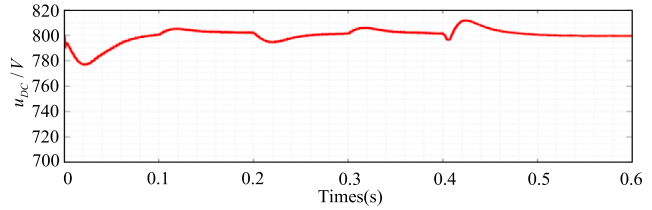


**Fig. 10.** DC bus voltage waveform.

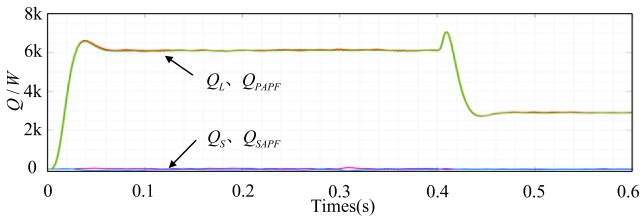


**Fig. 11.** Reactive power waveform without PAC.

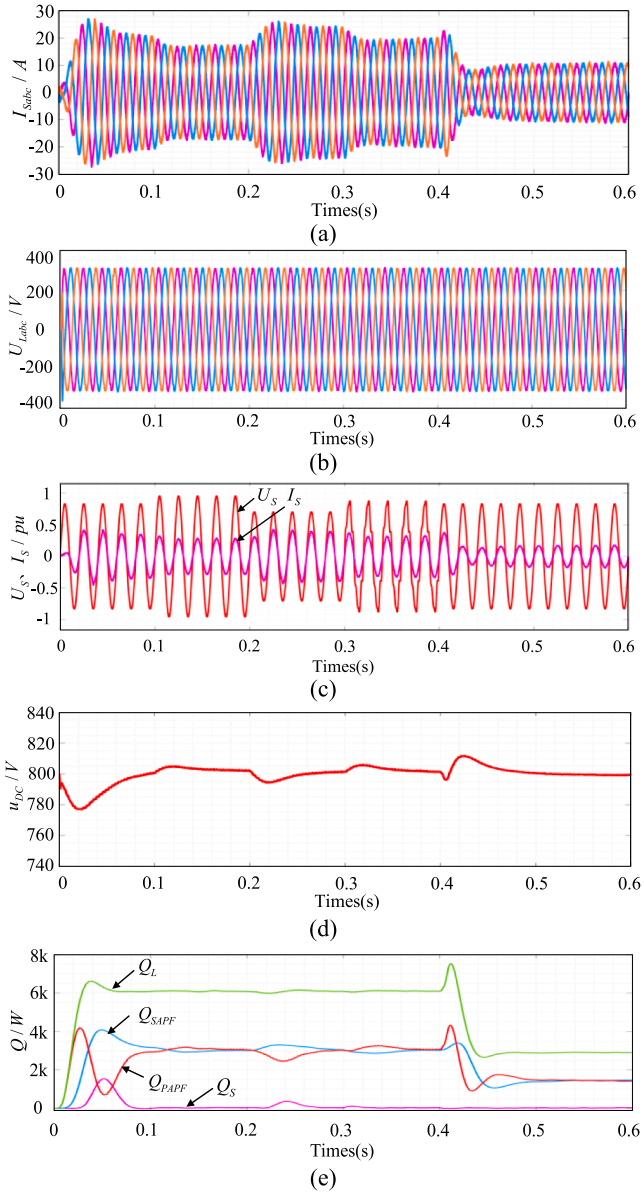


**Fig. 12.** UPQC compensation effect with PAC on the (a) grid current, (b) load voltage, (c) grid voltage and current phase, (d) DC bus voltage, and (e) reactive power waveforms.

and current for the three algorithms under various operating conditions is illustrated in Fig. 13. PDCS-PAC exhibits the lowest voltage and current harmonic components. Irrespective of system conditions, including temporary voltage fluctuations, harmonics, or sudden load changes, the proposed control strategy maintains the THD of voltage and current below 5%, satisfying the grid entry standard.

We compare the proposed strategy with existing literature based on

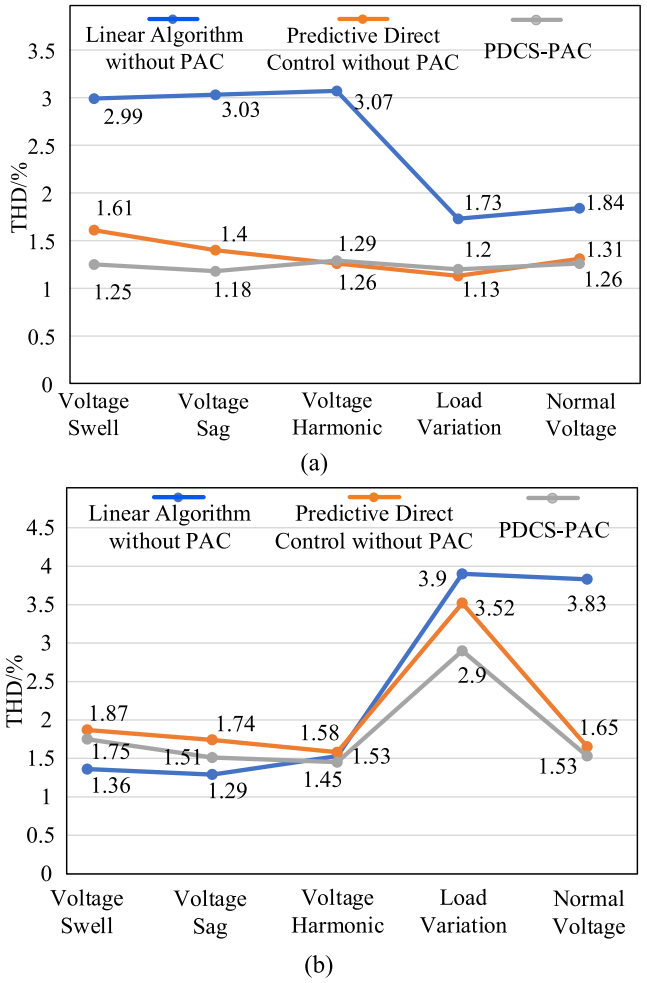


**Fig. 13.** Semi-physical experimental platform to compare (a) voltage THD and (b) current THD.

the FCS-MPC predictive indirect control algorithm without PAC and the non-linear sliding mode algorithm under identical parameter conditions [28,34]. The comparative analysis is presented in Table 2. verifying the superiority of the proposed algorithm.

## 5. Physical analysis

To validate the accuracy of the simulation outcomes, we construct an experimental platform (Fig. 14) to corroborate the proposed PAC-based UPQC predictive direct control strategy. For the hardware-in-the-loop semi-physical verification, we employ the HDSP-DF28335P real controller to generate pulses. The primary circuit model was built on a Typhoon HIL402 system. The system voltage and current harmonic distortion rate were analyzed using a HIOKI power quality analyzer PQ3198. The relevant parameters of the main circuit are detailed in Table 1.

**Table 2**
THD comparison of other control algorithms.

| THD/ % | Type of working operation | Non-linear sliding mode | Prediction indirect control | PDCS-PAC |
|---|---|---|---|---|
| Voltage | Voltage swell | 2.45 | 2.09 | 0.58 |
| | Voltage sag | 2.38 | 1.94 | 0.55 |
| Current | Before load change | 2.42 | 2.17 | 0.63 |
| | After load change | 2.84 | 2.38 | 0.51 |

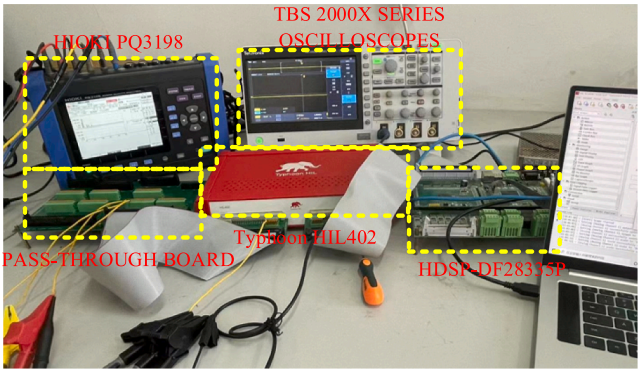


**Fig. 14.** Semi-physical experimental platform.

### 5.1. Performance of the PDCS-PAC under normal voltage conditions

The experimental findings when the three-phase grid input voltage is normal ($220\sqrt{2}$ V) are illustrated in Fig. 15. The PDCS-PAC effectively controls the grid-side power factor to 1 (Fig. 15(a)). The strategy maintains the load voltage at the set reference value $220\sqrt{2}$ V and controls the phase deviation of the load and grid voltages (Fig. 15(b)). The SAPF and PAPF do not engage in active power compensation, and the load's active power is solely supplied by the grid (Fig. 15(c)). The load's reactive power is equally distributed between the two inverters in the PAC-based UPQC system, with no reactive power sourced from the grid (Fig. 15(d)). The harmonic distortion rates of the grid currents before and after compensation are presented in Fig. 15(e) and (f). Due to the impact of the non-linear load, the grid experiences substantial harmonic distortion. Following compensation by the PDCS-PAC, the THD of the grid current declines from 23.59% to 2.34%, ensuring the stability of the grid current.

### 5.2. Performance of the PDCS-PAC under harmonic voltage condition

Experimental results under harmonics (14%) in the three-phase grid input voltage are exhibited in Fig. 16. The PDCS-PAC effectively maintains the grid power factor to 1 under harmonic voltage conditions and retains the sinusoidal waveform of load voltage with constant amplitude, maintaining a stable voltage on the user side. The SAPF and PAPF

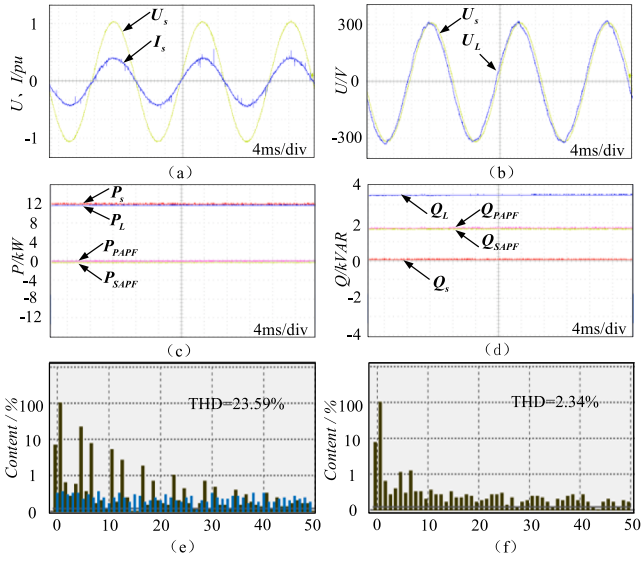


**Fig. 15.** Normal voltage condition. (a) Grid voltage and current phase; (b) grid voltage and load voltage phase; (c) active power; (d) reactive power, (e) compensates the front grid current, and (f) grid current after compensation.

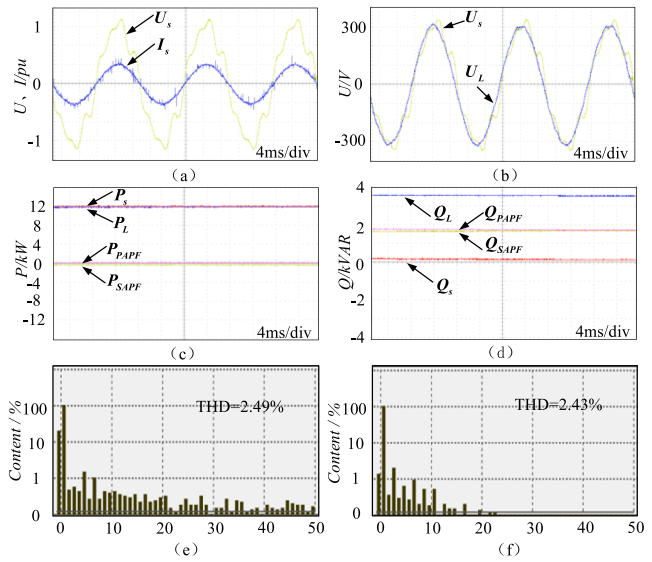


**Fig. 16.** Harmonic voltage condition. (a) Grid voltage and current phase, (b) grid voltage and load voltage phase, (c) active power, (d) reactive power, (e) grid current after compensation, and (f) load voltage after compensation.

supply the load reactive power and the load's fully active power is provided by the grid (Fig. 16(c) and (d)). Following PDCS-PAC's compensation, the THDs of the grid current and load voltage are reduced to 2.49% and 2.43%, respectively, maintaining system stability (Fig. 16 (e) and (f)).

### 5.3. Performance of the PDCS-PAC under dual operating conditions of voltage harmonics and swell

Experimental outcomes of the three-phase grid with voltage swell (10%) and the presence of harmonics (14%) are illustrated in Fig. 17. Although the swell and harmonics increase and distort the grid voltage, the load voltage maintains constant sinusoidal wave amplitude under PDCS-PAC (Fig. 17(b)). The proposed strategy (Fig. 17(a)) exhibits no impact of the supply voltage fluctuation on the power factor on the network side. In addition, an active flow between SAPF and PAPF exists under voltage fluctuations, and the grid supplies the load active power (Fig. 17(c)). Both inverters supply the load reactive power and the grid does not supply reactive power (Fig. 17(d)). Following the compensation of PDCS-PAC, the THD of grid current and load voltage are 2.55% and 2.63%, respectively, enhancing the system's power quality issue (Fig. 17(e) and (f)).

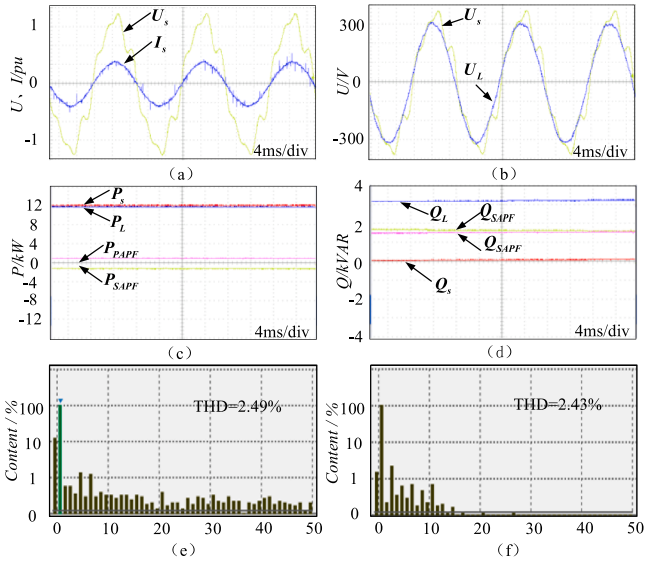


**Fig. 17.** Harmonic and swell dual condition. (a) Grid voltage and current phase, (b) grid voltage and load voltage phase, (c) active power, (d) reactive power, (e) grid current after compensation, and (f) load voltage after compensation.

### 5.4. Performance of the PDCS-PAC under dual operating conditions of voltage harmonics and sag

Experimental results during a voltage drop (10%) in the three-phase grid and a harmonic voltage (14%) are illustrated in Fig. 18. Although quality issues exist with the supply-side voltage due to sag and harmonics (Fig. 18(a) and (b)), the grid current and load voltage maintain a constant sinusoidal wave amplitude under the control of the PDCS-PAC-based UPQC strategy, and the system power factor is always 1. During voltage fluctuations, an active power exchange occurs between the two PAC-based UPQC inverters, and simultaneous reactive power is supplied to the load, without the grid contributing to the load's reactive power compensation (Fig. 18(c) and (d)). Following the compensation by PDCS-PAC, the THD of grid current and load voltage are 2.43% and 2.71%, respectively, enhancing the system's power quality issue (Fig. 18 (e) and (f)).

### 5.5. Performance of the PDCS-PAC under changing load conditions

Experimental results of the load variation condition are illustrated in Fig. 19, where the UPQC connected non-linear load changes from R = 20 Ω and L = 50 mH to R = 40 Ω and L = 10 mH. The current input to the grid varies with load variation (Fig. 19(a) and (b)). In addition, the proposed PDCS-PAC strategy can maintain the stable amplitude of the sinusoidal load voltage (Fig. 19(c)–(f)). It also exhibits the input current on the grid side as a sinusoidal wave controls the grid voltage and current in the same phase, and retains the system power factor as 1. The PAPF and SAPF supply the reactive power required by the load, relieving the reactive power burden on PAPF and enhancing SAPF utilization.

This study computes the harmonic distortion rate THD for various operating conditions before and after compensation of the UPQC system, as detailed in Table 3.

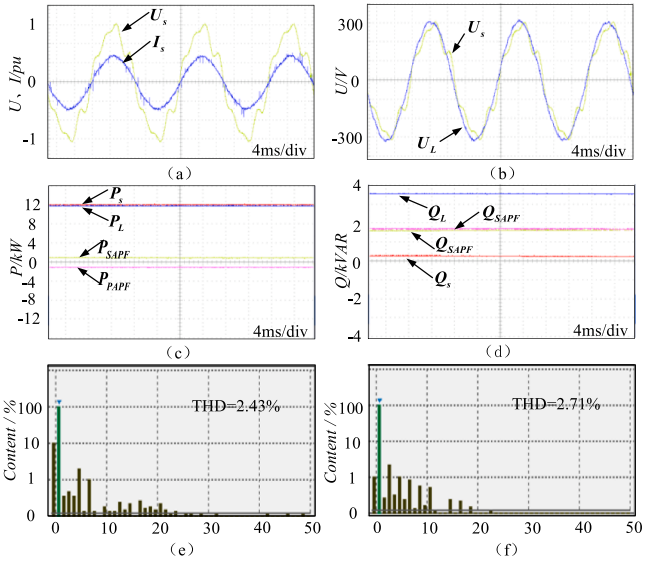


**Fig. 18.** Harmonic and sag dual conditions. (a) Grid voltage and current phase, (b) grid voltage and load voltage phase, (c) active power, (d) reactive power, (e) grid current after compensation, and (f) load voltage after compensation.

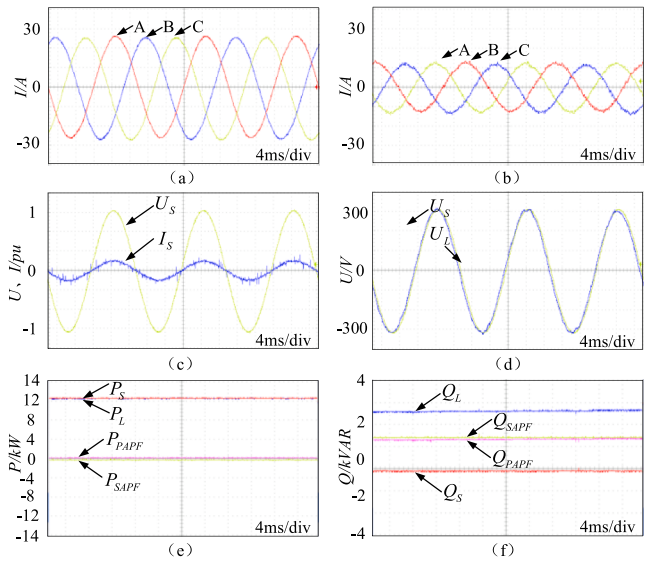


**Fig. 19.** Changing load conditions. Grid current (a) before and (b) after load change. (c) Grid voltage and current phase. (d) Grid voltage and load voltage phase. (e) Active power. (f) Reactive power.

**Table 3**
THD before and after system compensation.

| Voltage condition types | Before compensation THD/% | | After compensation THD/% | |
|---|---|---|---|---|
| | Load voltage | Grid current | Load voltage | Grid current |
| Harmonics + Rise | 13.67 | 23.53 | 2.63 | 2.55 |
| Harmonics + Sag | 14.16 | 23.52 | 2.71 | 2.43 |
| Harmonics | 14.00 | 23.42 | 2.43 | 2.49 |
| Normal | 0.10 | 23.59 | 2.54 | 2.34 |
| Load change | 0.10 | 25.01 | 2.67 | 4.24 |

## 6. Conclusion

This study proposes a prediction direct control strategy for PAC-based UPQC. The strategy simplifies the controller structure, alleviates the control algorithm's complexity, and optimizes the power distribution of the UPQC series and parallel converters using the equal sharing principle of reactive power. Real-time simulation and experimental results validate the efficacy and feasibility of the strategy. In addition, comparative analysis with the linear algorithm and the predictive direct control strategy without PAC indicates that the proposed strategy relieves the reactive power burden on the PAPF, enhances SAPF utilization, and demonstrates good voltage-current harmonic management performance.

## CRediT authorship contribution statement

**Guifeng Wang:** Conceptualization, Methodology, Validation, Supervision, Funding acquisition. **Zewen Wu:** Formal analysis, Investigation, Resources, Writing – original draft. **Zhan Liu:** Writing – review & editing, Data curation, Visualization, Project administration.

## Declaration of Competing Interest

The authors declare that they have no known competing financial interests or personal relationships that could have appeared to influence the work reported in this paper.

## Data availability

Data will be made available on request.

## Acknowledgments

We thank LetPub for its linguistic assistance during the preparation of this manuscript. This work was supported by the National Natural Science Foundation of China under Grant 51707086.

## References

[1] Lpez-Martn VM, Azcondo FJ, Pigazo A. Power quality enhancement in residential smart grids through power factor correction stages. IEEE Trans Ind Electron Nov. 2018;65(11):8553–64.
[2] Hussain I, Agarwal RK, Singh B. MLP control algorithm for adaptable dual-mode single-stage solar PV system tied to three-phase voltage-weak distribution grid. IEEE Trans Ind Informat Jun. 2018;14(6):2530–8.
[3] Igual R, Medrano C. Research challenges in real-time classification of power quality disturbances applicable to microgrids: A systematic review. Renew. Sustain. Energy Rev., vol. 132, Oct. 2020.
[4] Zhang H, Sun CD, Li ZX, Liu J, Cao HY, Zhang X. Voltage vector error fault diagnosis for open-circuit faults of three-phase four-wire active power filters. IEEE Trans Power Electron Mar. 2017;32(3):2215–26.
[5] Dharmakeerthi CH, Mithulananthan N, Saha TK. Impact of electric vehicle fast charging on power system voltage stability. Int J Electr Power Energy Syst 2014; 57:241–9.
[6] Zhao X, Zhang C, Chai X, Zhang J, Liu F, Zhang Z. Balance control of grid currents for UPQC under unbalanced loads based on matching-ratio compensation algorithm. J Mod Power Syst Clean Energy Nov. 2018;6(6):1319–31.
[7] Jin J, Li H, Yang R, Li Y, Zhou Q, Feng G, et al. An improved compensation method for voltage sags and swells of the electric vehicles charging station based on a UPQC-SMES system. Int J Electr Power Energy Syst Dec. 2022;143.
[8] Sarita K, Sachin K, Vardhan Aanchal Singh S, Madurai ER, Saket RK, Shafiullah GM, et al. Power enhancement with grid stabilization of renewable energy-based generation system using UPQC-FLC-EVA technique. IEEE Access, Nov 2020;8:207443–64.
[9] Wang J, Sun K, Wu H, Zhu J, Xing Y, Li Y. Hybrid connected unified power quality conditioner integrating distributed generation with reduced power capacity and enhanced conversion efficiency. IEEE Trans Ind Electron Dec. 2021;68(12): 12340–52.
[10] da Silva SAO, Campanhol LBG, Pelz GM, de Souza V. Comparative performance analysis involving a three-phase UPQC operating with conventional and dual/inverted power-line conditioning strategies. IEEE Trans Power Electron Nov. 2020; 35(11):11652–65.
[11] Modesto RA, da Silva SAO, de Oliveira AA, Bacon VD. A versatile unified power quality conditioner applied to three-phase four-wire distribution systems using a dual control strategy. IEEE Trans Power Electron Aug. 2016;31(8):5503–14.
[12] Zhao X, Liu Y, Chai X, Guo X, Wang X, Zhang C, et al. Multimode operation mechanism analysis and power flow flexible control of a new type of electric energy router for low-voltage distribution network. IEEE Trans Smart Grid Sept. 2022;13(5):3594–606.
[13] Patel Ashish, Mathur HD, Bhanot Surekha. An improved control method for unified power quality conditioner with unbalanced load. Int J Electr Power Energy Syst 2018;100:129–38.
[14] Xu Y, Xiao X, Sun Y, Long Y. Voltage sag compensation strategy for unified power quality conditioner with simultaneous reactive power injection. J Mod Power Syst Clean Energy Jan. 2016;4(1):113–22.
[15] Patel Ashish, Mathur Hitesh Datt, Bhanot Surekha. Enhancing VA sharing between the shunt and series APFs of UPQC with a modified SRF-PAC method. IET Power Electron 2020;13(2):275–85.
[16] Osaloni OO, Saha AK. Voltage dip/swell mitigation and imaginary power compensation in low voltage distribution utilizing improved Unified power quality conditioner (I-UPQC). JERA Jun. 2020;49:84–103.
[17] Ni F, Wo S, Li Z. Coordinated control strategy of UPQC by dynamic collaborative task-solving scheme based on multi-agent system. Energy Syst Jan. 2022;13: 215–33.
[18] Khadkikar V, Chandra A. A new control philosophy for a unified power quality conditioner (UPQC) to coordinate load-reactive power demand between shunt and series inverters. IEEE Trans Power Del Oct. 2008;23(4):2522–34.
[19] Huang X, Fan Z, Miao S, Xu D, Lu W, Ma Z. Coordinated power control strategy of unified power quality conditioner with energy storage unit. High Voltage Eng Oct. 2018;44(10):3390–8.
[20] Fagundes SM, Cardoso FL, Stangler EV, Neves FAS, Mezaroba M. A detailed power flow analysis of the dual unified power quality conditioner (iUPQC) using power angle control (PAC). Electric Power Syst Research Mar. 2021;192:106933.
[21] Liu X, Wang D, Peng Z. An improved finite control-set model predictive control for nested neutral point-clamped converters under both balanced and unbalanced grid conditions. Int J Electr Power Energy Syst Jan. 2019;104:910–23.
[22] Baier CR, Ramirez RO, Marciel EI, Hernández JC, Melín PE, Espinosa EE. FCS-MPC without steady-state error applied to a grid-connected cascaded H-Bridge multilevel inverter. IEEE Trans Power Electron Oct. 2021;36(10):11785–99.

[23] Mohapatra SR, Agarwal V. An improved reduced complexity model predictive current controller for grid-connected four-leg multilevel inverter. IEEE Trans Ind Appl 2020;56(1):498–506.
[24] Guo L, Jin N, Gan C, Luo K. Hybrid voltage vector preselection-based model predictive control for two-level voltage source inverters to reduce the common-mode voltage. IEEE Trans Ind Electron Jun. 2020;67(6):4680–91.
[25] Chakrit P, Kongpol A, Phonsit S. Harmonic mitigation in electric railway systems using improved model predictive control. Energies Apr. 2021;14(7).
[26] Ferreira SC, Gonzatti RB, Pereira RR, da Silva CH, da Silva LEB, Lambert-Torres G. Finite control set model predictive control for dynamic reactive power compensation with hybrid active power filters. IEEE Trans Ind Electron Mar. 2018;65(3):2608–17.
[27] Khan I, Vijay AS, Doolla S. Nonlinear load harmonic mitigation strategies in microgrids: state of the art. IEEE Syst J Sept. 2022;16(3):4243–55.
[28] Liu T, Wang H, Ge L, Wang S. Power quality integrated regulator compensation strategy based on FCS-MPC. Power Syst Technol Sept. 2019;43(9):3377–84.
[29] Kotturu J, Kothuru S, Agarwal P. Simplified predictive control of unified power quality conditioner. In: 2018 9th IEEE Int. Symp. Power Electron. Distrib. Gener. Syst., Charlotte, NC, USA, pp. 1-6; 2018.
[30] Luo Y, Wang S, Yang D, Zhou B, Liu T. Direct prediction compensation strategy of unified power quality conditioner based on FCS-MPC. IET Gener Transm Distrib Jul. 2020;14(22):5020–8.
[31] Vinothkumar V, Kanimozhi R. RETRACTED ARTICLE: Power flow control and power quality analysis in power distribution system using UPQC based cascaded multi-level inverter with predictive phase dispersion modulation method. J Ambient Intell Human Comput, Jun 2021;12:6445–63.
[32] Cortes P, Rodriguez J, Silva C, Flores A. Delay compensation in model predictive current control of a three-phase inverter. IEEE Trans Ind Electron Feb. 2012;59(2):1323–5.
[33] Kumar Panda Anup, Patnaik Nishant. Management of reactive power sharing & power quality improvement with SRF-PAC based UPQC under unbalanced source voltage condition. Int J Electr Power Energy Syst 2017;84:182–94.
[34] Patjoshi RK, Mahapatra K. High-performance unified power quality conditioner using non-linear sliding mode and new switching dynamics control strategy. IET Power Electron Jun. 2017;10(8):863–74.

Guifeng Wang received the B.S. and M.S. degrees from School of Information and Electrical Engineering at the China University of Mining and Technology, Xuzhou, China, in 2004 and 2007, respectively. He received his Ph.D. degree in Power Electronics and Electrical Drive from Shanghai Jiao Tong University, Shanghai, China. He is presently working as a Senior Engineer in the School of Electrical Engineering and Automation, Jiangsu Normal University, Xuzhou, China. His current research interests include power electronic converters for electrical drives and power quality.

Zewen Wu was born in Jiangsu, China in 1998. He received the B.S. degree in Nanjing University of Science and Technology Zijin College, Nanjing, China, in 2020. He is currently pursuing the master's degree in School of Electrical Engineering and Automation, Jiangsu Normal University, Xuzhou, China. His current research interests include power electronic converters for electrical drives and power quality.

Zhan Liu received the B.S., M.S. and Ph.D. degrees from School of Information and Electrical Engineering at the China University of Mining and Technology, Xuzhou, China, in 2004, 2007, and 2016, respectively. He is presently working as a Faculty Member in the School of Electrical Engineering and Automation, Jiangsu Normal University, Xuzhou, China. His current research interests include power electronics, modern control theory and multilevel converters.